Mapping key soil micronutrients across the Tibetan Plateau

Huangyu Huo[1,2], Xiling Gu[1,2], Jiayi Li[1,2], Shanshan Yang[1], Yafeng Wang[1*], Jinzhi Ding[1*]

[1]State Key Laboratory of Tibetan Plateau Earth System, Environment and Resources (TPESER), Institute of Tibetan Plateau Research, Chinese Academy of Sciences, Beijing 100101, China.

[2]University of Chinese Academy of Sciences, College of Resources and Environment, Beijing 100049, China.

**Corresponding to:* Jinzhi Ding (jzding@itpcas.ac.cn), Yafeng Wang (yfwang@itpcas.ac.cn)

Abstract. Soil micronutrients supply sustains critical ecological functions but exhibit poorly quantified distribution patterns in high-altitude ecosystems. This study bridges this knowledge gap through a large-scale investigation across the Tibetan Plateau, a cold-arid region where cryogenic weathering, aridity, and suppressed pedogenesis interact to govern micronutrient cycling. We assembled a plateau-wide dataset from 526 sites with triplicate surface soils (0-10 cm) per site (n = 1,660). Seven micronutrients (Fe, Mn, Cu, Zn, Ni, V, Mo) were measured and paired with multi-source predictors (climate, vegetation, soil properties, topography, graze disturbance, and weathering proxy). Elemental contents span broad ranges, with site-level summaries (mean ± SD, mg·kg^{-1}) of Fe 22,864.30 ± 7,589.01, Mn 576.74 ± 206.44, Cu 25.32 ± 9.28, Zn 27.24 ± 8.55, Ni 49.35 ± 10.98, V 56.99 ± 19.33, and Mo 4.63 ± 1.14. Random Forest model was employed to quantify controls and generate high-resolution spatial maps. Key results reveal that pronounced regional heterogeneity driven primarily by climate-related weathering intensity and topography variable, with secondary modulation from soil and vegetation factors. Element-specific spatial patterns were observed, with Fe enrichment in southeastern/southern plateaus, Mn gradients increasing southeastward and Cu over the western-northern plateau with minima in the southeast. Zn hotspots in central-eastern and western marginal zones, Ni enriched across the northern-central interior and western highlands, and V exhibits a moderate spatial gradient, with higher contents in the southeastern Tibetan Plateau and relatively lower values in the northwest. Mo weakly patterned, slightly higher on northern basins and lower toward the southeast. We provide 1-km maps of all seven micronutrients together with pixel-wise uncertainty layers to support benchmarking of process-based micronutrient cycling models and to inform sustainable ecosystem management under climate change. The dataset is openly available at TPDC (https://doi.org/10.11888/Terre.tpdc.303049; Huo et al., 2025).

1 Introduction

As essential yet trace-level components of living systems, micronutrients (e.g., Fe, Mn, Cu, Zn, Ni, V, Mo) sustain fundamental ecological processes, including photosynthesis (Fe, Mn; Fischer et al., 2015; Schmidt et al., 2020), respiration (Fe; Dallman, 1986), enzymatic/redox functions (Cu, Zn, Mn, V; Hänsch et al., 2009), and biological nitrogen fixation (Ni, V, Mo; O'Hara, 2001). Crucially, micronutrient gradients in soils propagate through trophic chains, directly influencing human nutrition and health; deficiencies exacerbate global malnutrition burdens (Fageria et al., 2002; White et al., 2005). Despite their pivotal role in ecosystem stability and food security (Presteele et al., 2016; Stehfest et al., 2019), critical knowledge gaps persist regarding the distribution patterns and drivers of soil micronutrients from regional to global scales.

Soil micronutrient supply originates from coupled physicochemical weathering and biological mediation, critically regulated by local climate and topography (Ochoa-Hueso et al., 2020; Hartmann et al., 2023). In cold-arid high-altitude regions, particularly the Tibetan Plateau, extreme environmental interactions uniquely govern micronutrient cycling. Cryogenic processes such as glacial erosion and freeze-thaw cycles, accelerate physical bedrock weathering to mobilize lithogenic micronutrient reservoirs, while aridity concurrently constrains chemical weathering and elemental release (Mu et al., 2020; Mu et al., 2016). Low temperatures suppress biological turnover and synergize with aridity to compromise pedogenesis through clay deficits and diminished mineral reactive sites, thereby reducing elemental retention capacity (Dijkstra et al., 2004). These counteracting processes fundamentally shape micronutrients distribution patterns, yet remain severely understudied. Current research is largely restricted to localized transects (e.g., Heihe River Basin, Tibetan Plateau Highway) with limited spatial representation (Zhang et al., 2012; Guan et al., 2017; Bu et al., 2016).

To address these knowledge gaps, we conducted a large-scale field investigation across the Tibetan Plateau, establishing 526 sampling sites distributed across representative temperature and moisture gradients (Fig. 1). The sampling design encompassed the plateau's dominant vegetation types and lithological classes. Using this dataset, we analyzed distribution patterns and key controlling factors for seven essential micronutrients (Fe, Mn, Cu, Zn, Ni, V, Mo). We then applied a Random Forest algorithm to generate high-resolution spatial distribution maps of these micronutrients, representing the first comprehensive quantification at this scale and resolution.

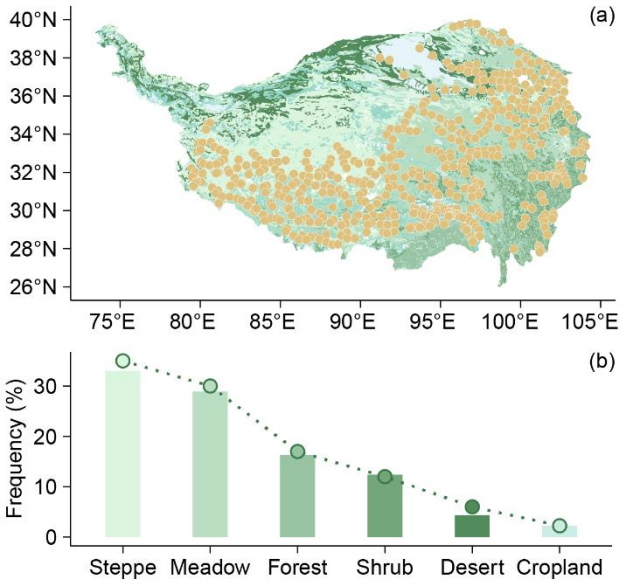

Figure 1. Sampling strategy and ecosystem representativeness. (a) Spatial distribution of sampling sites superimposed on China's 1:1,000,000 vegetation map. (b) Areal proportions of ecosystem types (bars) versus sampling point frequency distribution (dots) across corresponding ecosystems. Similar bar and dot heights indicate that the sampling is proportionally representative.

2 Methods

2.1 Field survey and soil micronutrients analysis

We analyzed 1,660 topsoil samples collected from 526 locations during a 2019-2021 growing season (July-August) field survey across the Tibetan Plateau (79-105°E, 27-40°N; **Fig. 1a**). Sampling sites represent major plateau ecosystems: forests, shrubs, steppes, meadows, deserts, and croplands (**Table 1**). The sites span broad environmental gradients, ranging from 759 to 5565 m in elevation, −7.83 to 18.46 °C in mean annual temperature (MAT), and 23 to 898 mm in mean annual precipitation (MAP), effectively capturing the plateau's topographic and climatic variability. Site was selected using standardized criteria: maintaining relative homogeneity in species composition, community structure, and habitat conditions, and avoiding proximity to roads or areas with frequent human activity. At each location, we established a 15 m transect collecting triplicate soil samples (0-10 cm depth) at 0 m, 7.5 m, and 15 m positions. This depth was chosen because it represents the biologically active surface horizon most relevant to plant uptake and microbially mediated cycling, and is widely used in regional soil inventories for comparability across ecosystems. On the Tibetan Plateau, steppes and meadows constitute the dominant land cover, so most samples correspond to mineral A horizons; in forested sites, the 0-10 cm layer may include an organic-rich surface. This consistent protocol ensures cross-site comparability while capturing the variability of surface layer that most strongly interacts with vegetation and climate. Geographic coordinates, elevation, community type, and species composition (Cheng et al., 2022) were systematically documented.

To ensure the reliability of soil micronutrient measurements, we adopted a two-step analytical strategy. First, in situ measurements were conducted using a second-generation portable Niton X-ray fluorescence (XRF) analyzer to obtain preliminary contents under natural field conditions. However, because this instrument could not reliably detect Mo, all soil samples were subsequently air-dried, sieved (2 mm), and re-analyzed in the laboratory using a third-generation XRF. Compared with the second-generation device, the third-generation XRF offers an extended detection range and improved accuracy (Lemière, 2018). All data presented in this study are based on the laboratory XRF measurements.

To further validate the laboratory XRF results, a subset of 218 samples was randomly selected and re-analyzed using Inductively coupled plasma-Mass Spectrometry (ICP-MS), a widely accepted reference method (Simon, 2005). The two methods showed strong correlations for Fe, Mn, Cu and V (R^2 = 0.67-0.89, P<0.001), with values closely aligning with the 1:1 line, indicating reliable quantification. For Zn and Ni, XRF and ICP-MS results were also significantly correlated, though systematic deviations from the 1:1 line were observed (**Fig. S1**). XRF tended to slightly over- or underestimated absolute contents of Zn and Ni contents compared with ICP-MS. To address this, we calibrated Zn and Ni, using the regression relationships between the two methods and then repeated spatial mapping. For Mo, the results obtained from the two methods were not fully consistent, likely due to its low content. Comparative results of both methods are provided in the Supplementary Information (**Figs. S2-S4**).

Table 1. Ecosystem classification and sampling coverage on the Tibetan Plateau.

Biome	Characteristics and dominant plant species	elevation ranges	climate conditions (temperature/ precipitation)	No. of samples	No. of locations
Steppe	Alpine steppes, dominated by cold-adapted herbaceous species such as *Stipa purpurea*, features sparse vegetation adapted to cold-arid conditions.	1961-5151 m	-7.1-8.0 ℃; 34.32-785.61 mm	569	180
Meadow	Alpine meadows feature dense, low-stature vegetation sustained by year-round low temperatures, high humidity, and water-retentive soils. These ecosystems thrive on gentle slopes and valley floors at higher elevations, hosting relatively diverse flora with characteristic dominance of sedges including *Kobresia pygmaea* and *K. humilis*.	2661-5565 m	-7.8-9.2 ℃; 158.42-848.70 mm	499	154
Forest	Forests on the Tibetan Plateau concentrate primarily in the southeastern region, dominated by high-altitude cold-temperate coniferous forests. These humid-adapted ecosystems feature *fir (Abies)* and *spruce (Picea)* species as characteristic components.	1453-4237 m	-0.6-16.5 ℃; 400.34-898.48 mm	265	87
Shrub	Tibetan shrublands primarily occur in arid and alpine zones, characterized by low-growing, drought-tolerant dwarf shrubs such as *Lonicera (honeysuckle)* and *Rhododendron* species adapted to nutrient-poor soils and extreme climatic conditions.	2169-5022 m	-5.2-11.8 ℃; 301.40-868.63 mm	190	64

Desert	Alpine deserts occur in extremely arid, cold regions and exhibit extremely sparse vegetation dominated by *arid-tolerant dwarf shrubs* and *herbs*.	2108-5158 m	-7.1-5.6 ℃; 22.64-443.43 mm	101	29
Cropland	Cropland, concentrated in river valleys and basin floors and is dominated by highland barley (*Hordeum vulgare* var. *nudum*, "qingke"), with spring wheat (*Triticum aestivum*), rapeseed (*Brassica napus*), and potato (*Solanum tuberosum*) commonly cultivated; vegetation cover is strongly seasonal and often bare after harvest.	759-4360 m	0.5-18.4 ℃; 112.53-783.06 mm	36	12

Biomes are grouped by diagnostic characteristics; dominant plant species are italicized. Elevation range gives the minimum-maximum elevation (m) of sampling sites within each biome. Climate conditions report site-level ranges of mean annual temperature (°C) and mean annual precipitation (mm). No. of samples is the number of soil samples analyzed (0-10 cm, three replicates per site), and No. of locations is the number of unique sampling sites.

2.2 Soil Properties

Soil samples were sifted through 2 mm sieve, discarding visible stones and extracted roots. Soil pH was measured using the potentiometric method, and soil texture analysis, quantifying clay, silt, and sand content fractions, was determined using a laser diffraction particle size analyzer (Mastersizer 2000, Malvern, UK). The sieved samples were air-dried for elemental analysis. Soil organic carbon (SOC) content was quantified via the potassium dichromate oxidation method (Walkley-Black) with external heating. The chemical index of alteration (CIA) was calculated using the molar proportions of Al_2O_3, CaO*, Na_2O, and K_2O according to the formula: $CIA = [Al_2O_3 / (Al_2O_3 + CaO^* + Na_2O + K_2O)] \times 100$ (Fedo et al., 1995). The chemical index of alteration reflects the relative loss of mobile base cations (Ca, Na, K) compared with the enrichment of immobile Al during weathering (McLennan, 1993). Higher chemical index of alteration values indicate stronger chemical weathering and more advanced soil development, whereas lower values suggest weaker weathering and limited leaching of base cations (Nesbitt et al., 1982).

2.3 Environmental variables

We considered geographic, climatic, biological, and edaphic drivers. Field measurements provided location (longitude, latitude), slope, aspect and vegetation type. For the spatial prediction of micronutrient distributions, however, the gridded predictor variables (e.g., elevation, slope, aspect, vegetation cover) were derived from online datasets in order to upscale site-level observations to the Plateau scale. Slope and aspect data came from the National Tibetan Plateau Data Center (https://data.tpdc.ac.cn). The digital elevation model (DEM) data were collected from the Resource and Environment Science and Data Center (https://www. resdc.cn/). Climate variables, mean annual temperature (MAT) and mean annual precipitation (MAP) were downloaded from the Climate Data Store (https://cds.climate.copernicus.eu/#!/home). The Aridity Index (AI), calculated as mean annual precipitation/mean annual reference evapotranspiration, was obtained from the Global

Aridity Index dataset (Trabucco et al., 2018), where higher values indicate greater humidity. Vegetation types (Forest, Shrub, Meadow, Steppe, Desert, Cropland) followed the 1:1,000,000 China Vegetation Map classification (Hou, 2019). The normalized difference vegetation index (NDVI) data were obtained from an Earthdata Search (https://search.earthdata.nasa.gov/search). The net primary productivity (NPP) data were obtained from the study by Chen et al. (2023) and were calculated using the CASA model (Potter et al., 1993). The grazing activity data were obtained from statistical yearbooks. Based on the lithological data published by Dijkshoorn et al. in 2018, the rock types on the Tibetan Plateau were classified into acidic igneous rock (IA), acidic metamorphic rock (MA), clastic sedimentary rock (SC), carbonate rock (SO), aeolian facies rock (UE), and fluvial facies rock (UF).

2.4 Relative importance analysis and soil micronutrient mapping

Soil micronutrient measurements were preprocessed to detect and remove outliers exceeding the mean ± 3 standard deviations. After data screening, the retained sample sizes are: Fe 1654 (from 1660), Mn 1630 (from 1646), Cu 920 (from 946), Zn 1655 (from 1661), Ni 180 (from 181), V 857 (from 867), and Mo 120 (from 123). To evaluate the relative importance of predictors in explaining soil micronutrient variability across the Tibetan Plateau, we applied the random forest permutation importance (%IncMSE) to independently cross-validate the driver rankings. For spatial prediction, we developed seven area-wide random forest models (each comprising 500 trees) targeting Fe, Mn, Cu, Zn, Ni, V, and Mo contents. The models were trained using a suite of environmental predictors, including topographic features (DEM, slope, aspect), climate variables (MAT, MAP, AI), vegetation indices (NDVI, NPP), soil properties (texture, SOC, pH, CIA), and grazing intensity. Random forest was selected for its ability to model complex, nonlinear relationships and interactions among diverse types of predictors. Model hyperparameters were optimized using grid search combined with tenfold cross-validation. To assess model generalizability, we examined the extent to which the predictor parameter space in the validation set overlapped with that of the original training data. Model performance was evaluated by comparing predicted versus observed values using scatterplots (predicted on the x-axis, observed on the y-axis) following the method of Piñeiro et al. (2008), with models achieving strong predictive performance (R^2 = 0.6-0.7). The uncertainty layer is calculated as the inter-pixel variance among tree predictions. All statistical analyses were conducted using R version 3.4.4.

3 Results

3.1 Soil micronutrients contents

Across all sites, soil micronutrient contents varied widely, with mean value of 22,864.30 ± 7,589.01 for Fe (mean ± SD, $mg \cdot kg^{-1}$), 576.74 ± 206.44 for Mn, 25.32 ± 9.28 for Cu, 27.24 ± 8.55 for Zn, 49.35 ± 10.98 for Ni, 56.99 ± 19.33 for V, and

4.63 ± 1.14 for Mo. Coefficients of variation (CV = SD/mean) were 33% for Fe, 36% for Mn , 37% for Cu , 31% for Zn, 22% for Ni, 34% for V and 25% for Mo. Collectively, Fe and Mn dominate in absolute abundance, whereas Cu-Zn-Ni-V occur at tens of mg·kg⁻¹ and Mo remains low (~5 mg·kg⁻¹), indicating heterogeneous but orderly micronutrient levels across the Plateau (**Figs. 2 and S5**).

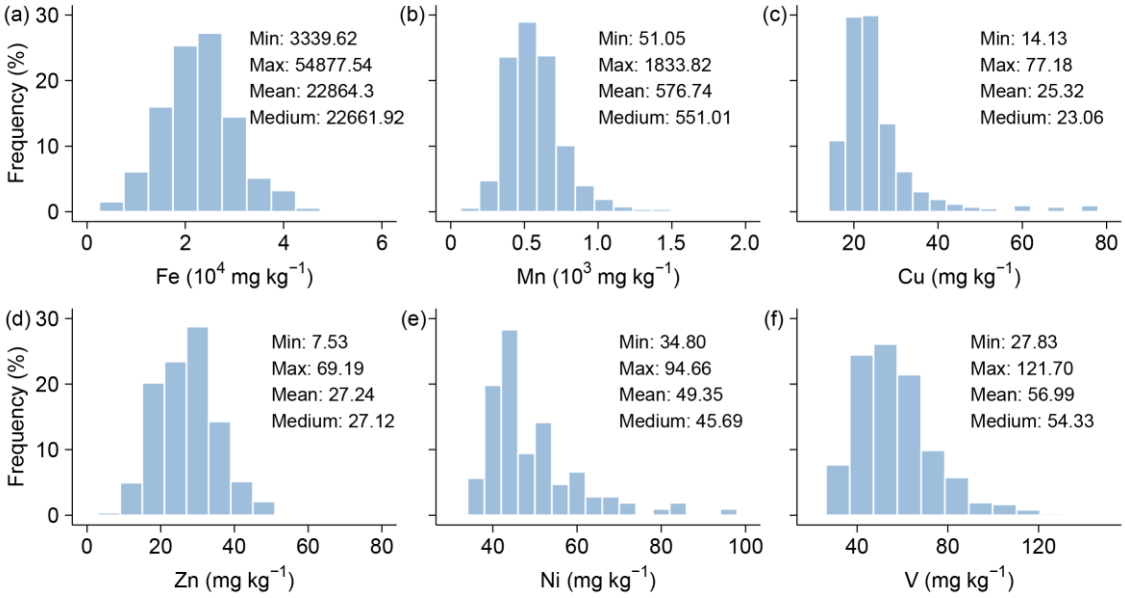

Figure 2. Frequency distributions of soil micronutrients (Fe, Mn, Cu, Zn, Ni, V) across the Tibetan Plateau.

3.2 Soil micronutrients across vegetation types

Soil micronutrients contents (Fe, Mn, Cu, Zn, Ni, V, and Mo) varied significantly among different vegetation types (**Figs. 3 and S6**). Fe contents were highest in shrub and forest ecosystems, with mean values of 26,264.11 mg·kg⁻¹ and 26,090.66 mg·kg⁻¹, respectively, significantly exceeding values observed in desert (19,762.66 mg·kg⁻¹) and steppe ecosystems (19,852.37 mg·kg⁻¹) by 31-33%. Similarly, Mn contents were greatest in forest (703.22 mg·kg⁻¹) and cropland (608.29 mg·kg⁻¹), followed by shrub (606.33 mg·kg⁻¹) and meadow (591.59 mg·kg⁻¹), while the lowest Mn levels were recorded in desert and steppe ecosystems (both below 510 mg·kg⁻¹).

Soil Cu showed minimal variation across vegetation types, with mean values ranging narrowly between 25.23 and 31.14 mg·kg⁻¹. Cropland had slightly higher Cu levels, but the differences were not statistically significant, suggesting a relatively uniform spatial distribution of Cu across ecosystems. Zn, however, demonstrated a strong vegetation-dependent variability, with the highest mean contents found in forest (32.00 mg·kg⁻¹) and shrub (31.15 mg·kg⁻¹) ecosystems. In contrast, Zn levels were markedly lower in steppe (22.94 mg·kg⁻¹) and desert (21.95 mg·kg⁻¹) soils, with differences exceeding 10 mg·kg⁻¹, indicating pronounced biogeochemical variation.

In contrast to the previous elements, Ni and Mo exhibited distinct patterns across vegetation types, with notably lower contents in forest and shrub ecosystems. Ni contents were highest in meadow soils (54.34 mg·kg^{-1}), followed by shrub (52.66 mg·kg^{-1}), steppe (48.78 mg·kg^{-1}), cropland (48.22 mg·kg^{-1}), desert (43.87 mg·kg^{-1}), and forest ecosystems (41.73 mg·kg^{-1}). Soil Mo contents showed negligible differences among ecosystems, though cropland exhibited marginally higher levels. No statistically significant differences were observed between vegetation types, indicating minimal vegetation control over Mo distribution.

The highest soil V mean value occurred in forest soils (63.70 mg·kg^{-1}), followed by shrub (61.94 mg·kg^{-1}) and cropland ecosystems (60.02 mg·kg^{-1}). These values were markedly greater than those observed in steppe (50.22 mg·kg^{-1}) and desert (52.80 mg·kg^{-1}) soils, with differences reaching up to 25%. Meadow soils showed intermediate V levels (56.07 mg·kg^{-1}). Statistical comparisons revealed that V contents in forest and shrub ecosystems were significantly higher than those in steppe and meadow ecosystems ($p < 0.05$).

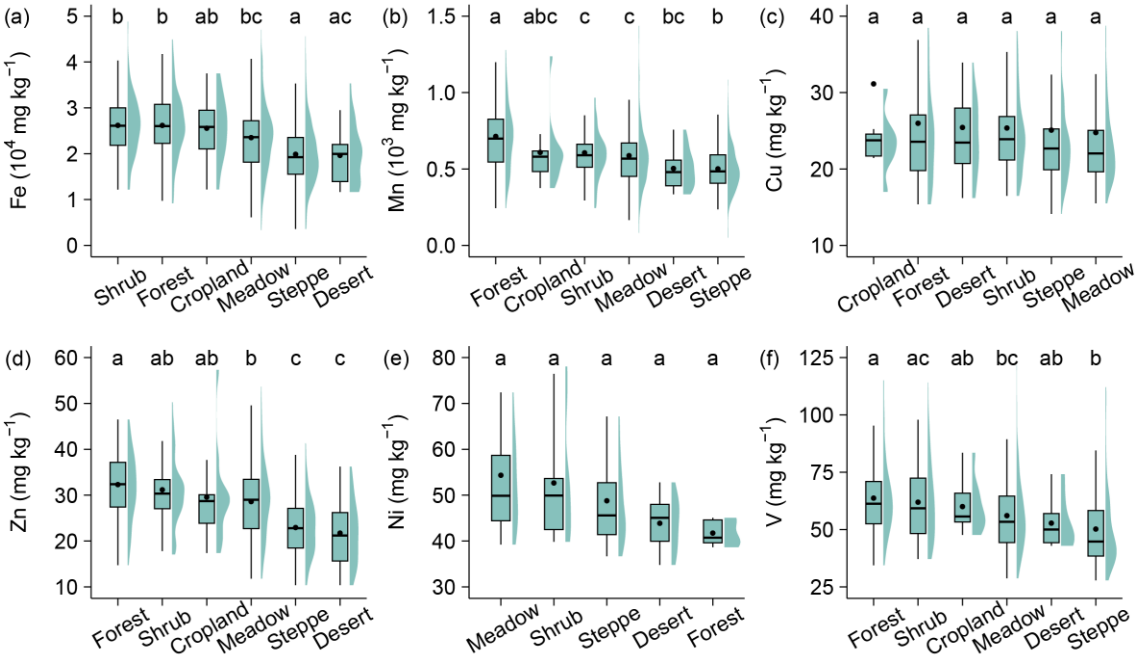

Figure 3. Variability in soil micronutrient contents (Fe, Mn, Cu, Zn, Ni, V) across Tibetan vegetation types. Boxplots show the data distributions for each vegetation type. Within each plot, the boxes represent the interquartile range (IQR), the horizontal lines within boxes indicate the median values, and black dots denote the mean values. The whiskers extend to 1.5 times the IQR. The surrounding shaded violin shapes indicate the kernel density distribution of the data. Lowercase letters denote significance groups from Tukey's HSD multiple comparisons ($\alpha = 0.05$): groups sharing at least one letter do not differ significantly, whereas groups with no letters in common differ significantly (e.g., "ab" is not different from "a" or "b").

3.3 Soil micronutrients across lithological classes

Lithological class exerted a significant influence on the spatial distribution of certain soil micronutrients (**Figs. 4 and S7**). Fe contents differed notably across lithological classes, with the highest values observed in soils derived from acidic

metamorphic rocks (mean value: 25,252.72 mg·kg⁻¹), followed by those from carbonate rocks (24,260.96 mg·kg⁻¹) and eolian facies rocks (23,902.77 mg·kg⁻¹). The lowest Fe contents were recorded in soils developed from acidic igneous rocks (20,830.15 mg·kg⁻¹). A similar geochemical pattern was observed for Mn, with the maximum contents in acidic-metamorphic-drived soils (658.37 mg·kg⁻¹), and the lowest in acidic-igneous-drived soils (530.45 mg·kg⁻¹).

Zn contents in soils also varied across lithologies, with the highest values associated with acidic metamorphic rocks (mean value of 30.79 mg·kg⁻¹), followed by eolian facies rocks and clastic sedimentary rocks, while relatively lower levels were found under acidic igneous rocks (25.27 mg·kg⁻¹) and fluvial facies rocks (25.10 mg·kg⁻¹). In contrast, Cu showed no significant differences among lithological classes. Cu contents were slightly higher under fluvial facies rocks (25.60 mg·kg⁻¹), but overall differences were minimal. Similarly, Mo contents were relatively uniform, with slightly elevated levels under acidic metamorphic rocks and eolian facies rocks (both ~4.86 mg·kg⁻¹), and lower values under clastic sedimentary rocks and carbonate rocks (both <4.48 mg·kg⁻¹), though differences were not statistically significant.

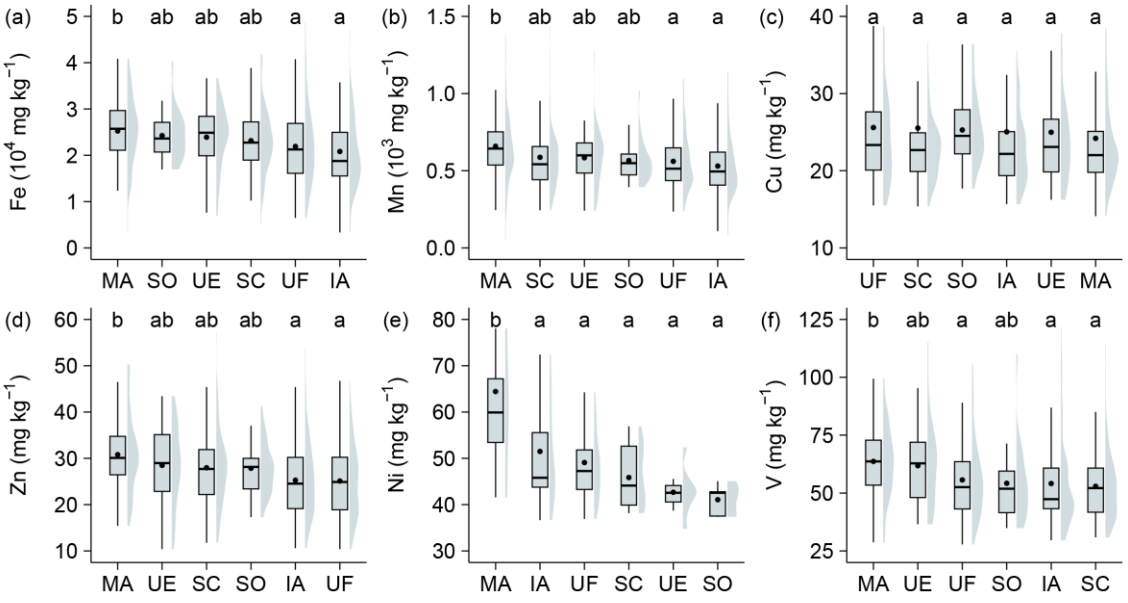

Figure 4. Variability in soil micronutrient contents (Fe, Mn, Cu, Zn, Ni, V) across Tibetan lithological classes. Boxplots show the data distributions for each lithological classes. Within each plot, the boxes represent the interquartile range (IQR), the horizontal lines within boxes indicate the median values, and black dots denote the mean values. The whiskers extend to 1.5 times the IQR. The surrounding shaded violin shapes indicate the kernel density distribution of the data. Lowercase letters denote significance groups from Tukey's HSD multiple comparisons ($\alpha = 0.05$): groups sharing at least one letter do not differ significantly, whereas groups with no letters in common differ significantly (e.g., "ab" is not different from "a" or "b"). Abbreviations of lithological classes: IA = acidic igneous rock, MA = acidic metamorphic rock, SC = clastic sedimentary rock, SO = carbonate rock, UE = eolian facies rock, UF = fluvial facies rock.

Soil Ni contents showed the most pronounced variation among lithologies, with the highest level recorded under acidic metamorphic rocks (64.43 mg·kg⁻¹), followed by acidic igneous rocks (51.49 mg·kg⁻¹). Soils developed from clastic sedimentary rocks and carbonate rocks had significantly lower Ni contents (45.85 and 41.06 mg·kg⁻¹, respectively). The

highest V contents were found in soils derived from acidic metamorphic rocks (63.67 $mg \cdot kg^{-1}$), followed by soils developed from eolian facies rocks (61.81 $mg \cdot kg^{-1}$) and fluvial facies rocks (55.67 $mg \cdot kg^{-1}$). In contrast, soils originating from carbonate (54.20 $mg \cdot kg^{-1}$), acidic igneous (54.11 $mg \cdot kg^{-1}$), and clastic sedimentary rocks (52.92 $mg \cdot kg^{-1}$) exhibited relatively lower V levels. In summary, Fe, Mn, Zn and V were substantially enriched in soils derived from acidic metamorphic rocks. Cu and Mo showed relatively uniform distributions across lithologies, Ni was notably elevated under acidic metamorphic rocks.

3.4 Drivers of soil micronutrient pattern

Relative importance analysis was conducted for five predictor groups, including climate, vegetation, soil properties, topography, and grazing disturbances. The rankings show clear element-specific controls (**Figs. 5a-f and S8**). Soil properties were the primary contributors to the spatial variation of micronutrient contents, followed by topographic and climatic factors, whereas vegetation and anthropogenic disturbance had relatively minor effects. Among all predictors, the chemical index of alteration, slope, and soil texture exhibited the highest importance, indicating that weathering intensity, terrain, and soil physical structure are the dominant controls on the spatial distribution of soil micronutrients. Specifically, the chemical index of alteration emerged as the dominant factor for Fe, Zn, and V. Topographic factors (slope) primarily influenced Mn, while climatic variables (MAP, AI) and biological productivity (NPP) contributed more to Cu and Ni variations. Mo is mainly influenced by the soil texture.

The partial dependence plots illustrated the nonlinear responses of seven soil micronutrients (Fe, Mn, Cu, Zn, Ni, V, and Mo) to five key environmental variables (**Figs. 6 and S9**). Overall, the effects of the chemical index of alteration, soil texture, slope, and aridity index varied substantially among elements. The chemical index of alteration showed a generally positive relationship with most micronutrients, particularly Fe, Mn, Zn, V, and Mo, which increased markedly when chemical index of alteration exceeded approximately 0.5. Soil texture exerted a moderate positive influence on micronutrients. In contrast, slope exhibited a saturating effect—nutrient concentrations rose sharply at low slope angles (<10°) and plateaued thereafter—highlighting the limited accumulation potential on steeper terrains. The aridity index demonstrated a clear U-shaped pattern for most micronutrients (Fe, Mn, Cu, Zn, Ni, V, and Mo), with relatively low concentrations under intermediate aridity. Seven micronutrients (Fe, Mn, Cu, Zn, Ni, V, and Mo) exhibited a typical U-shaped relationship with mean annual precipitation, showing higher contents in both low and high precipitation zones, and a clear trough in the intermediate range (approximately 300-500 millimeters). This pattern aligned closely with responses to drought indices, confirming shared moisture sensitivity. Collectively, these patterns emphasize that soil micronutrient distributions across the

Tibetan Plateau are strongly shaped by interactions among chemical weathering intensity, soil physical properties, and climatic aridity.

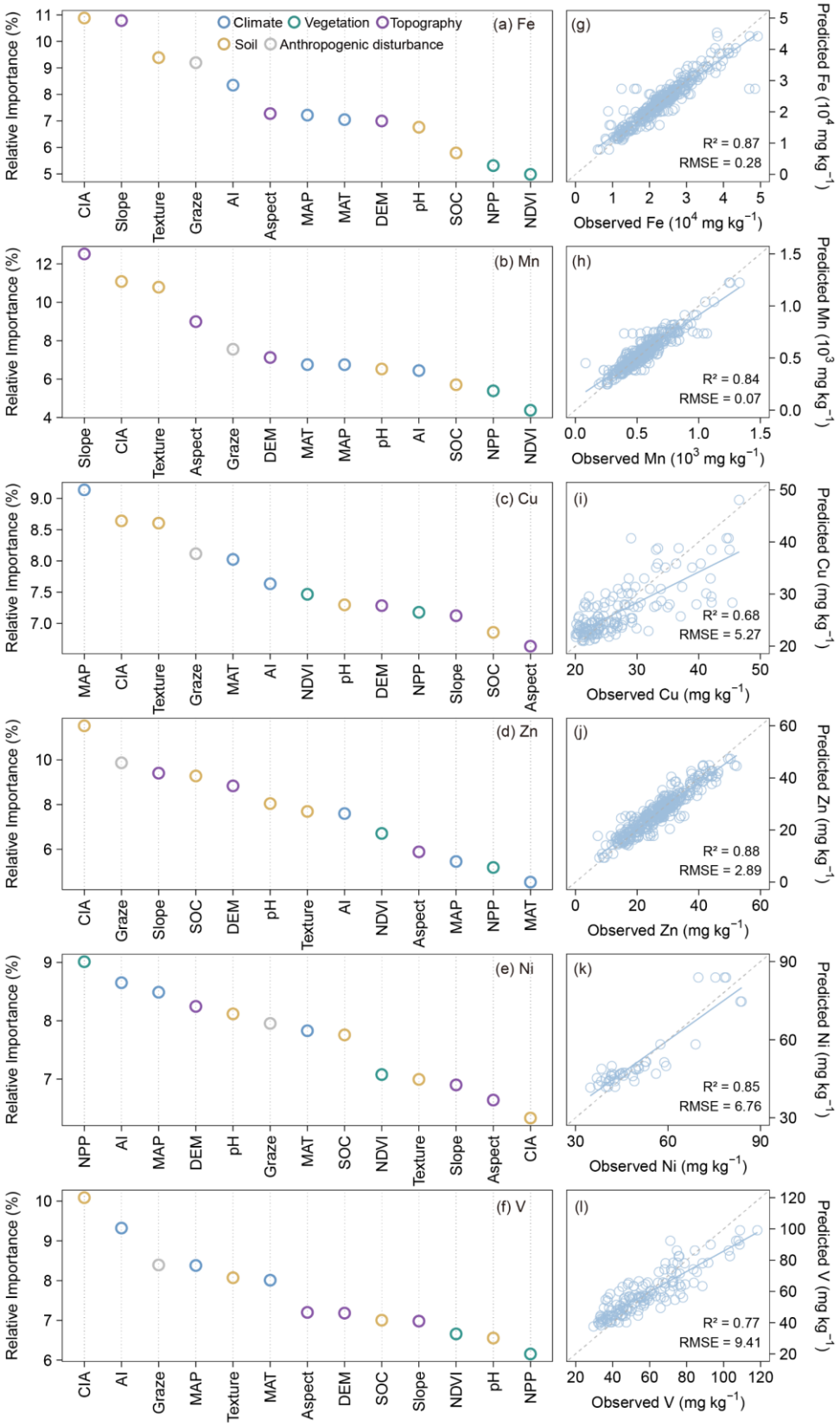

Figure 5. Relative importance of biotic and abiotic factors for soil micronutrients (Fe, Mn, Cu, Zn, Ni, V) on the Tibetan Plateau (a-f). Relationship between observed and predicted values of soil micronutrients (Fe, Mn, Cu, Zn, Ni, V) on the Tibetan Plateau based on the Random Forest model (g-l). The blue solid line represents the fitted relationship using ordinary least squares regression, while the gray dashed line indicates the 1:1 line between observed and predicted values.

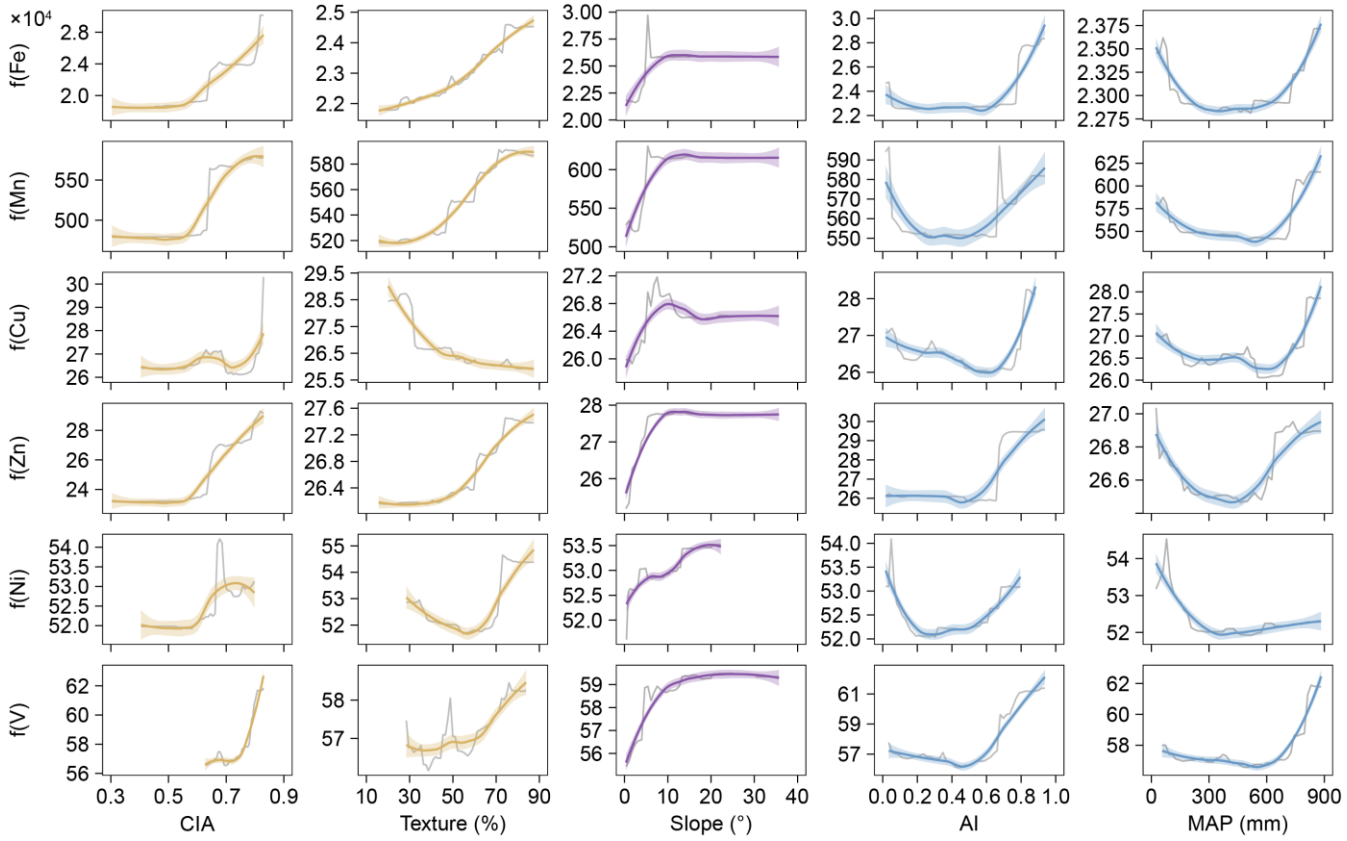

Figure 6. Partial dependence of six soil micronutrients (Fe, Mn, Cu, Zn, Ni, V) on four predictive variables: chemical index of alteration (CIA), Texture, Slope, aridity index (AI) and mean annual precipitation (MAP). Gray lines represent the original partial dependence, while smoothed fits for each micronutrient are shown as colored lines. Shaded areas represent the 95% confidence intervals.

3.5 Soil micronutrients maps

The random forest (RF) models exhibited strong overall predictive performance for soil micronutrient concentrations across the Tibetan Plateau, with varying accuracies among elements (**Figs. 5g-l and S8**). The models for Fe, Mn, Zn, Ni, and Mo performed best, with R^2 values ranging from 0.83 to 0.88 and relatively low RMSE, indicating high consistency between observed and predicted values. In particular, Zn (R^2 = 0.88) and Fe (R^2 = 0.87) achieved the highest predictive accuracy, suggesting that their spatial variability is well captured by the selected environmental predictors. Mo (R^2 = 0.83), Mn (R^2 = 0.84) and Ni (R^2 = 0.85) also showed strong model fits, reflecting robust representation of their spatial patterns. The Cu and V models displayed slightly lower but still acceptable performance (R^2 = 0.68 and 0.77, respectively), implying that additional predictors may be required to fully capture their local variability. Overall, these results demonstrate that the

248 random forest models effectively predict the spatial distributions of major soil micronutrients, with particularly high
249 reliability for Fe, Mn, Zn, and Ni.

250 **Figure 7 and Figure S10** illustrates the spatial patterns of soil micronutrients (Fe, Mn, Cu, Zn, Ni, V, and Mo) across the
251 Tibetan Plateau, as predicted by random forest models. The resulting maps reveal significant spatial heterogeneity of these
252 elements. The highest contents of Fe are primarily located in the southeastern region, the southern margins, and parts of the
253 western plateau. Mn shows a distinct gradient, with contents increasing from northeast to southwest. Predicted Mn values
254 range from 298.47 to 1,110.19 $mg \cdot kg^{-1}$, and the areas with the highest Mn contents are mainly distributed in the humid
255 southeastern and southern parts of the plateau. Cu ranges from 21.42 to 35.78 $mg \cdot kg^{-1}$, with relatively higher contents over
256 the western-northern interior and highlands and lower values in the humid southeastern valleys and along the southern
257 margin. Zn displays relatively high contents in the central-eastern region and along certain western edges of the plateau, with
258 predicted values ranging from 17.09 to 45.03 $mg \cdot kg^{-1}$. Ni has a narrower predicted content range (44.28-61.95 $mg \cdot kg^{-1}$) and
259 shows a more spatially homogeneous distribution. However, localized hotspots of elevated Ni contents are observed in parts
260 of the northeastern and southern plateau. Predicted V contents ranged from 40.79 to 82.00 $mg \cdot kg^{-1}$, displaying a clear spatial
261 gradient. Higher contents were predominantly found in the southeastern and southern regions of the plateau, where humid
262 climatic conditions and intense chemical weathering promote V enrichment. Moderate levels occurred across the central and
263 eastern plateau, while the lowest concentrations were observed in the arid western and northern areas. In contrast, Mo varies
264 within a narrower interval (3.88-5.87 $mg \cdot kg^{-1}$) and exhibits a weak plateau-wide gradient, with slight enrichment on the
265 northern plateau/basin areas and comparatively lower levels toward the southeast.
266

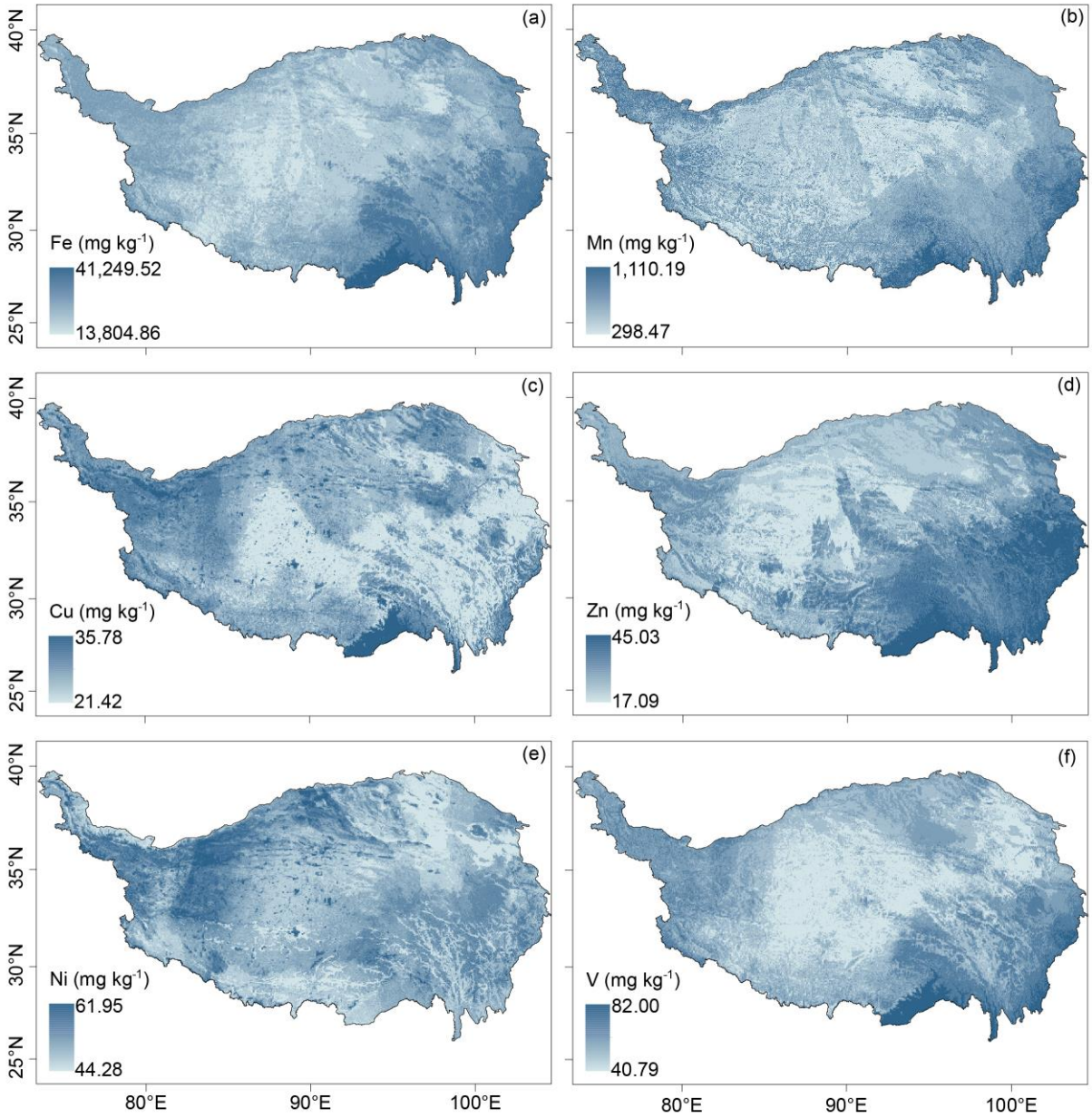

Figure 7. Spatial distribution of soil micronutrients (Fe, Mn, Cu, Zn, Ni, V) on the Tibetan Plateau.

4 Discussion

We added comparisons of our results with the few available observations on the Tibetan Plateau, as well as broader datasets from other regions, to better place our findings in a wider context (**Table S1**). In terms of data range and mean values, the contents and magnitudes of the soil micronutrients we observed are generally consistent with previous reports from the Plateau and global grassland soils, indicating the reliability of our datasets. For the Plateau, the mean Zn, and V contents in this study were slightly lower, while Ni were somewhat higher (**Fig. S11**). These discrepancies are more likely due to differences in study regions. Our sampling covered a much broader area, whereas previous studies focused mainly on local regions such as the Heihe Basin (Bu et al., 2016). Given the substantial spatial heterogeneity of soil micronutrients across the

Tibetan Plateau, such differences are expected and further highlight the necessity of exploring soil micronutrient patterns at the plateau scale.

The distribution of soil micronutrients across the Tibetan Plateau demonstrates significant spatial heterogeneity (**Figs. 2, 7, S4, and S10**), aligning with patterns observed in Europe for elements such as Zn (Van et al., 2023). This variability is predominantly governed by the interactions among soil, topography, and climate (**Figs. 5a-f, 6 S8 and S9**). Soils act as the principal sink for micronutrients entering the terrestrial environment through both natural processes and anthropogenic inputs. Consistent with continental-scale assessments, clay content emerged as the dominant control on the spatial distribution of soil Zn in Europe, with coarse-textured soils showing markedly lower Zn concentrations (Van et al., 2023). Similar texture effects have been reported for other elements: soil Cu is positively related to clay and negatively related to sand (Ballabio et al., 2018), sensitivity analyses show that soil Se increases with increasing clay (Jones et al., 2017), whereas surface-soil Hg decreases once sand exceeds ~30 % (Ballabio et al., 2021). These patterns agree with our observation that ecosystems developed on coarse substrates contain the lowest levels of micronutrients. This is because clay serves as an adsorption site for metal elements, whereas sandy soils are relatively weak adsorbents for micronutrients (Mesquita, 1998). In poorly developed soils with low clay content, such as those in arid climates, the lack of capacity to retain soil organic matter leads to a significant reduction in the amount of micronutrients, making them less likely to accumulate (Moreno-Jimenez et al., 2019). In addition to soil properties, factors such as topography also play a significant role in the micronutrient content of surface soils on the Tibetan Plateau. Eevation-related variations in soil micronutrient are limited, and some elements (e.g., Cu, Mo) remain relatively stable; Fe, Mn, Zn, and V show similar patterns, with higher contents at lower elevations than at higher ones (**Fig. S12 and S13**). Contents of Fe, Mn, Zn, and V increased with slope steepness, particularly below 10°, whereas Cu and Ni showed weaker or nonlinear trends. This pattern suggests that topography governs both physical and chemical soil-forming processes by controlling erosion, leaching, and moisture dynamics (Jenny, 1941; Montgomery, 2007). Steeper slopes enhance runoff and erosion, removing fine particles enriched in Fe and Mn oxides and promoting elemental redistribution along hillslopes, while also accelerating bedrock weathering and releasing lithogenic elements such as Fe and V (Yoo et al., 2006). In contrast, gentler slopes favor organic matter accumulation and reducing conditions that can immobilize or leach redox-sensitive elements. Overall, slope-driven variations in hydrology, weathering, and redox status collectively shape the spatial heterogeneity of soil micronutrients across the Plateau (Quesada et al., 2010).

Notably, precipitation emerges as the primary predictor for micronutrients such as Fe, Mn, Cu, Zn, V, and Mo, with all elements exhibiting characteristic U-shaped responses, with minima occurring at 300-500 mm. This pattern likely reflects distinct weathering regimes across precipitation gradients. In arid regions (<300 mm), physical weathering processes, including freeze-thaw fracturing and aeolian erosion, predominate, allowing micronutrients (e.g., Ni) to accumulate near the

surface due to evaporation effects (Pachauri et al., 2014; Moreno-Jimenez et al., 2023). In transitional precipitation regimes (300-500 mm), intensified chemical weathering occurs; however, leaching fluxes surpass the rates of parent material weathering, leading to soil elemental depletion (Anderson, 2019; Bluth et al., 1994; Hartmann et al., 2014). In humid regions (>500 mm), enhanced chemical weathering results in the formation of secondary clay minerals (e.g., montmorillonite, illite), whose negatively charged surfaces facilitate elemental retention through ionic adsorption and co-precipitation mechanisms (Alloway, 2009). To further verify these nonlinear effects, accumulated local effects (ALE) analyses were performed and revealed consistent U-shaped responses for Fe, Mn, Cu, Zn, V, and Mo, confirming the robustness of the partial dependence results (**Figs. S14 and S15**). This pattern likely reflects a trade-off between weathering intensity, leaching losses, and elemental retention under contrasting hydrological conditions. Additionally, MAP showed a significant positive correlation with the chemical index of alteration (**Fig. S16**), indicating that higher precipitation enhances chemical weathering. However, this relationship alone does not fully explain the observed U-shaped nutrient responses, as direct indicators of leaching fluxes and mineral retention are lacking. We therefore consider this U-shaped pattern, supported by multiple lines of evidence, as an open question for future investigation, emphasizing the need for complementary datasets (e.g., redox status, mineral composition) to refine its mechanistic interpretation. Although lithological differences are detectable for some elements, they do not alter the overall spatial patterns (**Figs. 4 and S7**). In summary, lithology modulates the baseline levels of certain micronutrients but is not the dominant factor shaping their regional distributions, which are more strongly governed by external environmental drivers such as climate, weathering intensity, sediment transport, and biotic cycling.

Our findings suggest that the aridity index is a significant determinant of soil micronutrient distribution. Specifically, elemental contents tend to decrease when the aridity index falls below a certain threshold (**Figs. 6 and S9**). This trend likely reflects reduced input or retention of elements under arid conditions. Grouped comparisons across aridity classes (humid, dry sub-humid, semi-arid, arid, and hyper-arid) were performed. The results show that the medians and means of Fe, Mn, Cu, Zn, Ni, V, and Mo decrease with increasing aridity, with the largest declines observed for Fe, Mn, Zn, and V (**Fig. S17 and S18**). Drought conditions may modify soil redox states, thereby influencing element speciation, adsorption capacity, mobility, and ultimately, leaching behavior (Brady et al., 2016; Loveland et al., 2003; Carter et al., 1995). Also, arid environments may indirectly impact micronutrients through alterations in soil pH and soil organic matter content (Moreno-Jimenez et al., 2019). Previous research has shown that droughts induced by climate change can restrict the availability of essential micronutrients, such as iron and zinc. This limitation, along with other adverse effects like diminished water availability, poses substantial threats to vital ecological processes and services in drylands, including food production (Gupta et al., 2008; Graham, 1991). Furthermore, ongoing regional warming and associated hydroclimatic shifts may interact with hydrology and redox

processes, organic-matter cycling, and vegetation patterns, thereby altering the availability and spatial variability of certain micronutrients (Myers et al., 2014; Pachauri et al., 2014).

Multiple biogeochemical processes are sensitive to micronutrient availability. Biological nitrogen fixation relies on Mo and Fe as essential cofactors of nitrogenase, while the methane cycle depends on Ni and Cu through their roles in methanogenesis and methane oxidation, respectively (Thauer et al., 2019; Stefan et al., 2020). Permafrost thaw and thermokarst development can further activate Fe-Mn redox cycling, altering metal mobility (Chauhan et al., 2024). Collectively, soil micronutrients depletion may cascade through nutrient cycling and ecosystem feedbacks, amplifying the impacts of ongoing environmental change across the Plateau.

5 Uncertainty

Although the laboratory XRF measurements used in this study were validated against ICP-MS and generally showed strong correlations, several limitations should be noted. For Fe, Mn, V and Cu, the two methods produced highly consistent results, supporting the robustness of the dataset. In contrast, Zn and Ni, exhibited systematic deviations from the 1:1 line, with XRF tending to slightly over- or underestimate contents relative to ICP-MS (**Fig. S1**). These deviations likely arise from element-specific detection sensitivities of XRF. To address this, we calibrated Zn and Ni, using the regression relationships between the two methods and then repeated spatial mapping. The results before and after calibration were not significantly different, confirming that these deviations do not affect our main findings (**Figs. S2 and S3**). For Mo, the results obtained from the two methods were not fully consistent, likely due to its low content (**Fig. S4**). The XRF-based measurements may involve considerable uncertainties. Nonetheless, we acknowledge that incorporating ICP-based measurements on a larger sample set would further strengthen the accuracy of the dataset, and future efforts should consider combining multiple analytical approaches to minimize methodological uncertainties.

Our random forest regression models demonstrated robust predictive capability (e.g. cross-validated R^2 range from 0.64 to 0.77 for Fe Mn Zn Ni; **Table S2**). Cu and Mo exhibit weaker predictive performance, which may be attributed to the following reasons: First, analytical limitations may introduce measurement error, as both elements occur at very low contents, especially Mo. Second, key process controls are not fully captured by the current predictors. E.g. Cu is strongly influenced by nonlinear interactions with Fe/Al oxides, whereas Mo is affected by carbonate content, redox conditions (Tack et al., 1995). These mineralogical and redox variables are underrepresented, leading to potential bias. In addition, both elements show hotspot-prone, right-skewed distributions (**Figs. 2 and S5**), likely due to localized anthropogenic sources. The spatial predictions inevitably contain uncertainties arising from both the Random Forest model and the input datasets. Model-based

uncertainty was quantified as the inter-tree variance among predictions (RF-SD; **Figs. S11 and S12**), while additional uncertainty may stem from sparse meteorological observations and limited soil sampling across the Tibetan Plateau. Nevertheless, model accuracy could be further improved to more extensive field sampling and refinement of input data. Specifically, targeted collection of soil micronutrient data and associated covariates in underrepresented high-altitude regions of the Tibetan Plateau is necessary to address existing spatial gaps. Additionally, systematic reduction of uncertainties inherent in gridded environmental datasets is essential, as these uncertainties propagate errors into micronutrient predictions. Continued advancement in both field observations and foundational geospatial dataset is crucial for improving the reliability of regional-scale element mapping.

We note that ecosystem-specific pedogenesis (e.g., organic-rich surface layers in some forests vs. thin mineral A horizons in grasslands) can contribute to differences in surface micronutrient contents. Consequently, part of the spatial variation we report likely reflects vertical horizon contrasts sampled at a uniform 0-10 cm depth. Users should consider this context when applying the dataset, especially for process inference or when comparing across ecosystems with contrasting surface horizons. Where applications require deeper profiles or horizon-specific interpretation, we recommend integrating our maps with local profile data.

6 Data availability

The gridded soil micronutrient (Fe, Mn, Cu, Zn, Ni, V, and Mo) maps for Tibetan Plateau can be downloaded from https://doi.org/ 10.11888/Terre.tpdc.303049 (Huo et al., 2025).

7 Conclusions

This study delivers a comprehensive assessment of spatial distribution patterns for seven soil micronutrients (Fe, Mn, Cu, Zn, Ni, V, and Mo) across the Tibetan Plateau, revealing pronounced regional-scale heterogeneity. Soil properties were the primary contributors to the spatial variation of micronutrient contents, followed by topographic and climatic factors, whereas vegetation and grazing disturbance had relatively minor effects. These findings highlight the coupled effects of climate, vegetation, and parent material on micronutrient biogeochemical cycling within the complex environmental context of the Tibetan Plateau. Using five predictor groups (climate, vegetation, soil properties, topography, and grazing disturbances), we generated high-resolution spatial maps for key soil micronutrients (Fe, Mn, Cu, Zn, Ni, V, and Mo) via machine learning. These maps provide validated initial conditions for process-based models simulating micronutrient cycling, advances understanding of elemental distribution in alpine ecosystems.

391 **Author contributions.**

392 JZ conceived the study. HY conducted the field survey and was responsible for data collection and processing. HY prepared
393 the manuscript with contributions from all co-authors.

394 **Competing interests.**

395 The contact author has declared that none of the authors has any competing interests.

396 **Acknowledgements.**

397 This study was supported by the Second Tibetan Plateau Scientific Expedition and Research Program (2022QZKK0101),
398 National Natural Science Foundation of China (42471159), and Chinese Academy of Sciences (CAS) Project for Young
399 Scientists in Basic Research (YSBR-037).

400 **Appendix A: Supplementary material**

401 **Appendix B: Metadata**

402 **References**

403 Alloway, B. J.: Soil factors associated with zinc deficiency in crops and humans, Environmental Geochemistry and Health,
404 31, 537-548, https://doi.org/10.1007/s10653-009-9255-4, 2009.
405 Anderson, S. P.: Breaking it down: Mechanical processes in the weathering engine, Elements: An International Magazine of
406 Mineralogy, Geochemistry, and Petrology, 15, 247-252, https://doi.org/10.2138/gselements.15.4.247, 2019.
407 Bluth, G. J., and Kump, L. R.: Lithologic and climatologic controls of river chemistry, Geochimica et Cosmochimica Acta,
408 58, 2341-2359, https://doi.org/10.1016/0016-7037(94)90015-9, 1994.
409 Ballabio, C., Jiskra, M., Osterwalder, S., Borrelli, P., Montanarella, L., and Panagos, P.: A spatial assessment of mercury
410 content in the European Union topsoil, Science of the Total Environment, 769, 144755, https://doi.org/
411 10.1016/j.scitotenv.2020.144755, 2021.
412 Ballabio, C., Panagos, P., Lugato, E., Huang, J. H., Orgiazzi, A., Jones, A., Fernández-Ugalde, O., Borrelli, P., and
413 Montanarella, L.: Copper distribution in European topsoils: An assessment based on LUCAS soil survey, Science of the
414 Total Environment, 636, 282-298, https://doi.org/10.1016/j.scitotenv.2018.04.268, 2018.

Brady, N. C. and Weil, R. R.: The nature and properties of soils, Pearson Education, Boston, 1104 pp., 2016.

Bu, J. W., Sun, Z. Y., Zhou, A. G., Xu, Y. N., Ma, R., Wei, W. H., and Liu, M.: Heavy Metals in Surface Soils in the Upper Reaches of the Heihe River, Northeastern Tibetan Plateau, China, 13, https://doi.org/ 10.3390/ijerph13030247, 2016.

Carter, M. R. and Stewart, B. A.: Structure and organic matter storage in agricultural soils, CRC Press, Boca Raton, 304 pp., 1995.

Chauhan, A., Patzner, M. S., Bhattacharyya, A., Borch, T., Fischer, S., Obst, M., Thomasarrigo, L. K., Kretzschmar, R., Mansor, M., Bryce, C., Kappler, A., and Joshi, P.: Interactions between iron and carbon in permafrost thaw ponds, Science of the Total Environment, 946, 174321, https://doi.org/10.1016/j.scitotenv.2024.174321, 2024.

Cheng, C. J., He, N. P., Li, M. X., Xu, L., Cai, W. X., Li, X., Zhao, W. W., Li, C., and Sun, O. J.: Plant species richness on the Tibetan Plateau: patterns and determinants, Ecography, 2023, https://doi.org/10.1111/ecog.06265, 2022.

Chen, J. H., Wang, Y. F., Sun, J., Zhang, J. X., Zhang, J. T., Wang, Y. X., Zhou, T. C., Huo, H. Y., and Liang, E. Y.: Linking ecosystem service benefit and grazing prohibition intensity can better optimize fence layout in northern Tibet, Land Degradation Development, 34, 2038-2051, https://doi.org/10.1002/ldr.4587, 2023.

Dallman, P. R.: Biochemical basis for the manifestations of iron deficiency, Annual Review of Nutrition, 6, 13-40, https://doi.org/10.1146/annurev.nu.06.070186.000305, 1986.

Dijkshoorn, J. A., van Engelen, V. W. P., and Huting, J. R. M.: Soil and landform properties for LADA partner countries (Argentina, China, Cuba, Senegal and The Gambia, South Africa and Tunisia), ISRIC Report 2008/06 and GLADA Report 2008/03, ISRIC-World Soil Information and FAO, Wageningen, 23 pp., 2008.

Dijkstra, J. J., Meeussen, J. C. L., and Comans, R. N. J.: Leaching of heavy metals from contaminated soils: an experimental and modeling study. Environmental Science & Technology, 38, 4390-4395, https://doi.org/10.1021/es049885v, 2004.

Fageria, N. K., Baligar, V. C., and Clark, R. B.: Micronutrients in crop production. Advances in Agronomy, 77, 185-268, https://doi.org/10.1016/S0065-2113(02)77015-6, 2002.

Fedo, C. M., Nesbitt, H. W., and Young, G. M.: Unraveling the effects of potassium metasomatism in sedimentary rocks and paleosols, with implications for paleoweathering conditions and provenance, Geology, 23, 921-924, https://doi.org/10.1130/0091-7613(1995)023<0921:UTEOPM>2.3.CO;2, 1995.

Fischer, W. W., Hemp, J., and Johnson, J. E.: Manganese and the evolution of photosynthesis, Origins of Life and Evolution of Biospheres, 45, 351-357, https://doi.org/10.1007/s11084-015-9442-5, 2015.

Graham, T. W.: Trace element deficiencies in cattle, Veterinary Clinice of North America-Food Animal Practice, 7, 153-215, https://doi.org/10.1016/S0749-0720(15)30816-1, 1991.

Gupta, U. C., Wu, K., and Liang, S.: Micronutrients in soils, crops, and livestock. Earth Science Frontiers, 15, 110-125, 2008.

Guan, Z. H., Li, X. G., and Wang, L.: Heavy metal enrichment in roadside soils in the eastern Tibetan Plateau, Environmental Science and Pollution Research, 25, 7625-7637, https://doi.org/ 10.1007/s11356-017-1094-8, 2017.

Hartmann, J., Moosdorf, N., Lauerwald, R., Hinderer, M., and West, A. J.: Global chemical weathering and associated P-release-The role of lithology, temperature and soil properties, Chemical Geology, 363, 145-163, https://doi.org/10.1016/j.chemgeo.2013.10.025, 2014.

Hartmann, M., and Six, J.: Soil structure and microbiome functions in agroecosystems, Nature Reviews Earth & Environment, 4, 4-18, https://doi.org/10.1038/s43017-022-00366-w, 2023.

Hänsch, R., and Mendel, R. R.: Physiological functions of mineral micronutrients (Cu, Zn, Mn, Fe, Ni, Mo, B, Cl), Current Opinion in Plant Biology, 12, 259-266, https://doi.org/10.1016/j.pbi.2009.05.006, 2009.

Hou, X. Y. (Ed.): Atlas of vegetation of China (1:1,000,000), Science Press, Beijing, 2019.

Jenny, H.: Factors of Soil Formation: A System of Quantitative Pedology, McGraw-Hill, New York, 1941.

Jones, D. L., Cross, P., Withers, P. J., DeLuca, T. H., Robinson, D. A., Quilliam, R. S., Harris, I. M., Chadwick, D. R., and Edwards-Jones, G.: Nutrient stripping: The global disparity between food security and soil nutrient stocks, Journal of Applied Ecology, 50, 851-862, https://doi.org/10.1111/1365-2664.12089, 2013.

Jones, G. D., Droz, B., Greve, P., Gottschalk, P., Poffet, D., McGrath, S. P., Seneviratne, S. I., Smith, P., and Winkel, L. H. E.: Selenium deficiency risk predicted to increase under future climate change, Proceedings of the National Academy of Sciences of the United States of America, 114, 2848-2853, https://doi.org/10.1073/pnas.1611576114, 2017.

Lemière, B.: A review of pXRF (field portable X-ray fluorescence) applications for applied geochemistry, Journal of Geochemical Exploration, 188, 350-363, https://doi.org/10.1016/j.gexplo.2018.02.006, 2018.

Lindsay, W. L.: Chemical equilibria in soils, John Wiley and Sons Ltd., New York, 449 pp., 1979.

Loveland, P. and Webb, J.: Is there a critical level of organic matter in the agricultural soils of temperate regions: a review, Soil Tillage Research, 70, 1–18, https://doi.org/10.1016/S0167-1987(02)00139-3, 2003.

McLennan, S. M.: Weathering and global denudation, The Journal of Geology, 101, 295-303, https://doi.org/10.1086/648222, 1993.

Mesquita, M. E.: Copper and zinc competitive adsorption in schistic and granitic acid soils, Agrochimica, 42, 235-245, 1998.

Montgomery, D. R.: Soil erosion and agricultural sustainability, Proceedings of the National Academy of Sciences of the United States of America, 104, 13268-13272, https://doi.org/10.1073/pnas.0611508104, 2007.

Moreno-Jimenez, E., Maestre, F. T., Flagmeier, M., Guirado, E., Berdugo, M., Bastida, F., Dacal, M., Díaz-Martínez, P., Ochoa-Hueso, R., Plaza, C, Rillig, MC., Crowther, T. W., and Delgado-Baquerizo, M.: Soils in warmer and less developed countries have less micronutrients globally, Global Change Biology, 29, 522-532, https://doi.org/10.1111/gcb.16478, 2023.

Moreno-Jimenez, E., Plaza, C., Saiz, H., Manzano, R., Flagmeier, M., and Maestre, F. T.: Aridity and reduced soil micronutrient availability in global drylands, Nature Sustainability, 2, 371-377, https://doi.org/10.1038/s41893--019-0262-x, 2019.

Mu, C. C., Zhang, F., Mu, M., Chen, X., Li, Z. L., and Zhang, T. J.: Organic carbon stabilized by iron during slump deformation on the Qinghai-Tibetan Plateau, Catena, 187, 104282, https://doi.org/10.1016/j.catena.2019.104282, 2020.

Mu, C. C., Zhang, T. J., Zhao, Q., Guo, H., Zhong, W., Su, H., and Wu, Q.B.: Soil organic carbon stabilization by iron in permafrost regions of the Qinghai-Tibet Plateau, Geophysical Research Letters, 43, 10286-10294, https://doi.org/10.1002/2016GL070071, 2016.

Myers, S. S., Zanobetti, A., Kloog, I., Huybers, P., Leakey, A. D., Bloom, A. J., Carlisle, E., Dietterich, L. H., Fitzgerald, G., Hasegawa, T., Holbrook, N. M., Nelson, R. L., Ottman, M. J., Raboy, V., Sakai, H., Sartor, K. A., Schwartz, J., Seneweera, S., Tausz, and M., Usui, Y.: Increasing CO_2 threatens human nutrition, Nature, 510, 139-142, https://doi.org/10.1038/nature13179, 2014.

Nesbitt, H.W., and Young, G.M.: Early Proterozoic climates and platemotions inferred frommajor element chemistry of lutites, Nature, 299, 715-717, https://doi.org/10.1038/299715a0, 1982.

Ochoa-Hueso, R., Plaza, C., Moreno-Jimenez, E., and Delgado-Baquerizo, M.: Soil element coupling is driven by ecological context and atomic mass, Ecology Letters, 24, 319-326, https://doi.org/10.1111/ele.13648, 2020.

O'Hara, G. W.: Nutritional constraints on root nodule bacteria affecting symbiotic nitrogen fixation: A review, Australian Journal of Experimental Agriculture, 41, 417-433, https://doi.org/10.1071/EA00087, 2001.

Pachauri, R. K., Allen, M. R., Barros, V. R., Broome, J., Cramer, W., Christ, R., Church, J. A., Clarke, L., Dahe, Q., and Dasgupta, P.: Climate change 2014: Synthesis report. Contribution of Working Groups I, II and III to the Fifth Assessment Report of the Intergovernmental Panel on Climate Change, IPCC, Geneva, Switzerland, 151 pp., 2014.

Piñeiro, G., Perelman, S., Guerschman, J. P., and Paruelo, J. M.: How to evaluate models:: Observed vs. predicted or predicted vs. observed? Ecological Modelling, 216, 316-322, https://doi.org/10.1016/j.ecolmodel.2008.05.006, 2008.

Potter, C. S., Randerson, J. T., Field, C. B., Matson, P. A., Vitousek, P. M., Mooney, H. A., and Klooster, S. A.: Terrestrial ecosystem production: A process model based on global satellite and surface data, Global Biogeochemical Cycles, 7, 811–841, https://doi.org/10.1029/ 93GB02725, 1993.

503 Prestele, R., Alexander, P., Rounsevell, M. D., Arneth, A., Calvin, K., Doelman, J., Eitelberg, D. A., Engström, K., Fujimori,
504 S., Hasegawa, T., Havlik, P., Humpenoeder, F., Jain, A. K., Krisztin, T., Kyle, P., Meiyappan, P., Popp, A., Sands, R. D.,
505 Schaldach, R., Schuengel, J., Stehfest, E., Tabeau, A., Van Meijl, H., Van Vliet, J., Verburg, P. H.: Hotspots of
506 uncertainty in land-use and land-cover change projections: A global-scale model comparison, Global Change Biology,
507 22, 3967-3983, https://doi.org/10.1111/gcb.13337, 2016.
508 Quesada, C. A., Lloyd, J., Schwarz, M., Patino, S., Baker, T. R., Czimczik, C., Fyllas, N. M., Martinelli, L., Nardoto, G. B.,
509 Schmerler, J., Santos, A. J. B., Hodnett, M. G., Herrera, R., Luizao, F. J., Arneth, A., Lloyd, G., Dezzeo, N., Kuhlmann,
510 I., Raessler, M., Brand, W. A., Geilmann, H., Moraes Filho, J. O., Carvalho, F. P., Araujo Filho, R. N., Chaves, J. E.,
511 Cruz Junior, O. F., Pimentel, T. P., and Paiva, R.: Variations in chemical and physical properties of Amazon forest soils
512 in relation to their genesis, Biogeosciences, 7, 1515-1541, https://doi.org/ 10.5194/bg-7-1515-2010, 2010.
513 Schmidt, W., Thomine, S., and Buckhout, T. J.: Iron nutrition and interactions in plants, Frontiers in Plant Science, 10, 1670,
514 https://doi.org/10.3389/fpls.2019.01670, 2020.
515 Simon M. N.: Inductively Coupled Plasma Mass Spectrometry Handbook, Blackwell Publishing, Oxford, 2005.
516 Stefan, B., Jiménez-Vicente, E., Echavarri-Erasun, C., and Rubio, L. M.: Biosynthesis of Nitrogenase Cofactors, Chemical
517 Reviews, 120, 4919-5794, https://doi.org/10.1021/acs.chemrev.9b00489, 2020.
518 Stehfest, E., van Zeist, W. J., Valin, H., Havlik, P., Popp, A., Kyle, P., Tabeau, A., Mason-D'Croz, D., Hasegawa, T., Bodirsky,
519 B. L., Calvin, K., Doelman, J. C., Fujimori, S., Humpenoeder, F., Lotze-Campen, H., van Meijl, H., and Wiebe, K.: Key
520 determinants of global land-use projections, Nature Communications, 10, 1-10,
521 https://doi.org/10.1038/s41467-019-09945-w, 2019.
522 St Clair, S. B. S., and Lynch, J. P.: The opening of Pandora's Box: Climate change impacts on soil fertility and crop nutrition
523 in developing countries, Plant and Soil, 335, https://doi.org/10.1007/s11104-010-0328-z101-115, 2010.
524 Tack, F.M., Verloo M.G.: Chemical speciation and fractionation in soil and sediment heavy metal analysis: a review,
525 International Journal of Environmental Analytical Chemistry 59, 225-238. https://doi:10.1080/03067319508041330,
526 1995.
527 Thauer, P. K.: Methyl (Alkyl)-Coenzyme M Reductases: Nickel F-430-Containing Enzymes Involved in Anaerobic Methane
528 Formation and in Anaerobic Oxidation of Methane or of Short Chain Alkanes, Biochemistry, 58, 5198-5220.
529 https://doi:10.1021/acs.biochem.9b00164, 2019.
530 Trabucco, A. and Zomer, R. J.: Global Aridity Index and Potential Evapo-Transpiration (ET0) Climate Database v2, CGIAR
531 Consortium for Spatial Information (CGIAR-CSI) [data set], https://cgiarcsi.community, 2018.

Van, Eynde. E., Fendrich, A. N., Ballabio, C., and Panagos, P.: Spatial assessment of topsoil zinc concentrations in Europe, Science of the Total Environment, 892, 164512, https://doi.org/10.1016/j.scitotenv.2023.164512, 2023.

White, P. J., and Broadley, M. R.: Biofortifying crops with essential mineral elements. Trends in Plant Science, 10, 586-593, https://doi.org/10.1016/j.tplan ts.2005.10.001, 2005.

Yoo, K., Amundson, R., Mudd, S. M., Sanderman, J., Amundson, R., and Blum, A.: Spatial patterns and controls of soil chemical weathering rates along a transient hillslope, Earth and Planetary Science Letters, 288, 184-193, https://doi.org/10.1016/j.epsl.2009.09.021, 2006.

Zhang, H., Wang, Z. F., Zhang, Y. L., and Hu, Z. J.: The effects of the Qinghai-Tibet railway on heavy metals enrichment in soils, Science of the Total Environment, 439, 240-280, https://doi.org/10.1016/j.scitotenv.2012.09.027, 2012.